Computer Simulations of Mesoscopic Plastic Deformation with Differential Geometric Forms for the Elastic Field of Parametric Dislocations : Review of Recent Progress

N.M. Ghoniem and J. Huang
Mechanical and Aerospace Engr. Dept., UCLA
Los Angeles, CA. 90095-1597, U.S.A.

N.M. Ghoniem and J. Huang
Mechanical and Aerospace Engr. Dept., UCLA
Los Angeles, CA. 90095-1597, U.S.A.
Tel. (310) 825-4866
Fax. (310)206-4830
e-mail: ghoniem@ucla.edu , jianming@seas.ucla.edu

Abstract. The elastic field of complex 3-D dislocation ensembles is described by differential geometric representations, which allow computer simulations of mesoscopic plastic deformation without additional ad hoc approximations for short-range dislocation reactions. The simple vector forms of differential geometry are independent of the coordinate system, and facilitate studies of dislocation generation, pileup formation, grain-boundary interaction, finite-length dipole nucleation and break-up, junction nucleation and destruction, interaction with defect clusters, and self-consistent boundary conditions. It is shown that the elastic field can be described in terms of simple combinations of three basic vectors and their dyadics in real and reciprocal space. These vectors are the unit tangent, Burgers vector, and unit radial vector between a source point on the dislocation and a field point. With the only limitation being dislocation cores interpenetrating up to one Burgers vectors, a review of recent progress and examples of the aforementioned short- and long-range dislocation reactions are given, with particular emphasis on computational issues of space and time resolution.

1. INTRODUCTION

Large-scale computer simulations of the collective behaviour of dislocation ensembles has steadily gained credence as a new tool for description of plasticity and fracture phenomena at length scales not amenable to analysis by atomistic or continuum methods. This approach represents a "missing link" in the array of experimental and computational techniques designed to understand and dissect the physical reasons for salient plasticity and material failure phenomena; such as heterogeneous material deformation, patterning and plastic flow localization, ductile-to-brittle transitions, and computational development of constitutive equations. Emerging applications of these techniques promise new computational tools for design and optimization of material systems in such diverse fields as electronic, opto-electronic, Micro-Electro-Mechanical (MEMS), and nuclear applications.

During the past decade, concerted efforts were focused on computational development of 3-d Dislocation Dynamics (DD), and have resulted in closing the gap between atomistic and continuum descriptions of plasticity (e.g. references [1-13], among others). At the present state of its development, approaches for 3-d DD computer simulations can be classed into three main categories: (1) lattice-based [1-3]; (2) force-based [4,7]; (3) differential stress-based [5,8]; and (4) parametric segment-based [6,9,10,12-15]. The primary distinction between these computational techniques resides in their treatment

of interaction forces between dislocations, self-forces on curved segments, and the variety of approximations in treating short-range reactions, boundary conditions and the precision in computing long-range forces. Similar to the Finite Element Method (FEM) of continuum mechanics, the Parametric Dislocation Dynamics (PDD) technique has been recently advanced to enable computational precision and flexibility in treating complex dislocation interactions in real materials [9,10,12-15]. In addition to the fast sum method for computations of elastic field variables [10], a rigorous formulation for the equations of motion [12] for generalized Degrees of Freedom (DOF) represent the foundations of PDD. However, PDD *applications* have been rather limited, thus requiring examples to illustrate the range of possibilities that can be realized with the method. More recent work has been aimed at the specific question of how accurately does the method deal with space and time resolution of complex dislocation processes [14]. A very simple and convenient form for the equations of the elastic field of parametric dislocation segments has also been recently obtained [15], which should be helpful to furthering investigations into a wide range of applications of PDD.

Our aim in this article is to give a concise *review* of the most recent developments of PDD, and in particular the new vector forms of the elastic field [15], and their application to the study of the most pertinent dislocation processes in DD simulations [16]. First, a differential geometry formulation of the elastic field variables is presented in section 2. This is followed by several examples, which illustrate the power as well as limitations of the method, are then highlighted in section 3. We show that the method can naturally capture all short- and long-range dislocation reactions without additional ad hoc assumptions, such as those made in 2-D DD simulations of the previous decade. Finally, summary and conclusions are discussed in section 4.

2. FORMULATION

Fig. (1) shows a schematic representation of a curved dislocation segment, which is described by a scalar parameter *w*. The segment is completely defined by the dependence of the position vector **P** on the scalar parameter. The radius vector **R** defines the relationship between a source point on the dislocation at **P** and a field point at **Q**. Now define the vectors: Burgers vector **b**, tangent vector **T**, unit tangent vector **t** and unit radius vector **e**:

$\mathbf{T} = \frac{d\mathbf{l}}{dw}$, $\mathbf{t} = \frac{\hat{\mathbf{O}}}{T}$, $\mathbf{e} = \frac{\mathbf{R}}{R}$, where **l** is the arc-length vector. We also define three Bravais vectors ($\mathbf{a}_1 = \mathbf{e}$ $\mathbf{a}_2 = \mathbf{t}$, $\mathbf{a}_3 = \mathbf{b}$) and their reciprocals: $\mathbf{a}^1 = \frac{1}{2pV}(\mathbf{a}_2 \times \mathbf{a}_3)$, $\mathbf{a}^2 = \frac{1}{2pV}(\mathbf{a}_3 \times \mathbf{a}_1)$, $\mathbf{a}^3 = \frac{1}{2pV}(\mathbf{a}_1 \times \mathbf{a}_2)$, where $V = (\mathbf{a}_1 \times \mathbf{a}_2) \cdot \mathbf{a}_3$

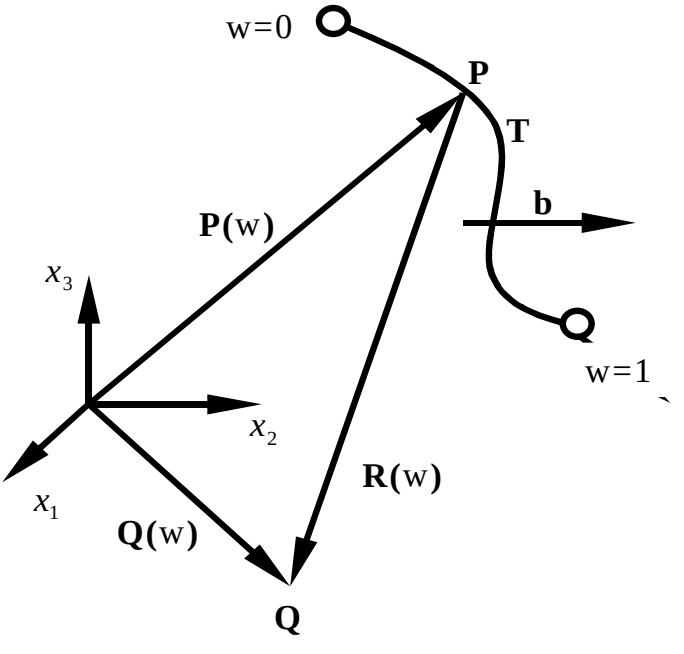

Fig. (1): Parametric representation of a general curved segment.

Differential forms for the elastic field variables of isotropic materials can be obtained from the Bravais vector triplet in real and reciprocal space [15]. For example, the displacement vector **u** and stress tensor **σ**, can be obtained by affine mappings of the scalar interval *dw* onto the vector interval *d***u** and second order tensor interval *d***σ**, respectively. Similarly, the differential interaction energy dE_{int} is obtained by mapping the scalar double differential $dw_I dw_{II}$ for two separate parametric dislocation segments. These affine mapping transformations can be written as [15]:

$$\frac{d\mathbf{u}}{dw} = \frac{T}{4R}\left\{\frac{(\mathbf{s}\times\mathbf{a}_1)\cdot\mathbf{a}_2}{p\,(1+\mathbf{s}\cdot\mathbf{a}_1)}\mathbf{a}_3 + \frac{V}{1-n}\left[(1-2n)\,\mathbf{a}^1\right] + \frac{1}{2p}\mathbf{a}_1\right\}$$

$$\frac{d\boldsymbol{\acute{o}}}{dw} = \frac{mVT}{2R^2}\left\{\frac{1}{1-n}\left(\mathbf{a}^1 \otimes \mathbf{a}_1 + \mathbf{a}_1 \otimes \mathbf{a}^1\right) + \left(\mathbf{a}^2 \otimes \mathbf{a}_2 + \mathbf{a}_2 \otimes \mathbf{a}^2\right) - \frac{1}{2p\,(1-n)}\left(\mathbf{a}_1 \otimes \mathbf{a}_1 + \mathbf{I}\right)\right\}$$

$$\frac{dE_{\text{int}}}{dw_I dw_{II}} = -\frac{mT_I T_{II}}{4p\,R}\left[\begin{array}{l}\left(\mathbf{a}_2^I \cdot \mathbf{a}_3^I\right)\left(\mathbf{a}_2^{II} \cdot \mathbf{a}_3^{II}\right) - \frac{1}{1-n}\left(\mathbf{a}_2^I \cdot \mathbf{a}_2^I\right)\left(\mathbf{a}_3^I \cdot \mathbf{a}_3^I\right) \\ + \frac{2n}{1-n}\left(\mathbf{a}_2^{II} \cdot \mathbf{a}_3^I\right)\left(\mathbf{a}_2^I \cdot \mathbf{a}_3^{II}\right) - \frac{1}{1-n}\left(\mathbf{a}_2^I \cdot \mathbf{a}_2^{II}\right)\left(\mathbf{a}_3^I \cdot \mathbf{a}_1\right)\left(\mathbf{a}_3^{II} \cdot \mathbf{a}_1\right)\end{array}\right]$$

(1)

In Eqn. (1), μ is the shear modulus, ν Poisson's ratio, **I** the unit tensor, and **s** is an arbitrary unit vector. The equation can be easily programmed to obtain the total field arising from many curved segments by straightforward quadrature sums [10], which is standard in FEM formulations. EOM for the generalized coordinates **P**, **T** and **N** (normal vector) are then obtained from variational principles and the segment is parametrically reformulated after each integration time step [12]. The elastic field of simple dislocation geometry (e.g. infinitely straight or circular loops, and finite straight segments) can be easily obtained by integration with respect to the scalar parameter *w* [15]. The form of Eqn. (1), which is different from standard textbook expressions that are based on Burgers equation [16], is quite convenient for 3-d computations, because it is vector-based, does not involve higher order tensor components, and independent of the coordinate system.

3. DISLOCATION REACTIONS

In this section, we present results of computer simulations for some of the most salient dislocation mechanisms that are involved in large-scale simulations of mesoscopic plastic deformation.

3.1 Generation

Dislocation generation by the Frank-Read (F-R) mechanism has been extensively studied during the past decade, and is generally considered a good test of newly developed computational techniques. Nonetheless, issues of computational accuracy and resolution have not been systematically investigated. Fig. (2) displays a projection on the (111) plane in FCC Cu for the time evolution of the dislocation line of an F-R source that is activated on the same glide plane. A uniaxial impact stress σ_{11} =50 MPa along [100] is suddenly applied, and corresponds to a critical resolved shear stress (CRSS) of $\frac{t}{m} = 0.041\%$. The dislocation mobility is taken as M=10^4 Pa^{-1} s^{-1}, while E=50 GPa and ν=0.31. All distances are measured in units of the lattice constant *a* (0.36 nm for Cu).

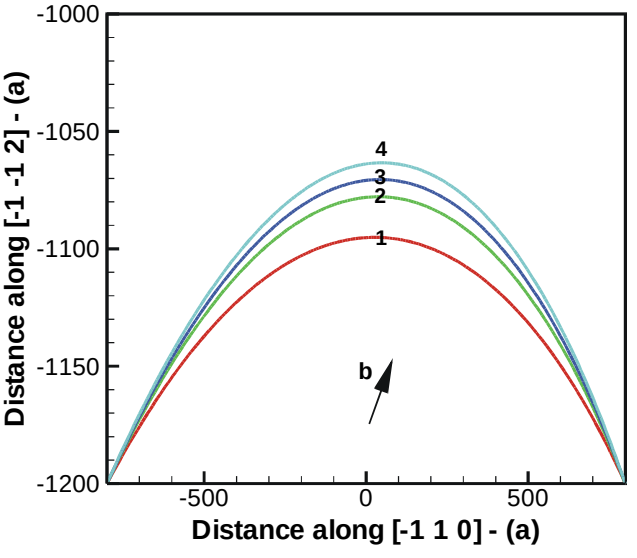

Fig. (2): Time evolution of an F-R source in FCC Cu at the intervals: (1) 10ps, (2) 20ps, (3) 30ps, and (4) equilibrium state. F-R source **b** = [-1 0 1].

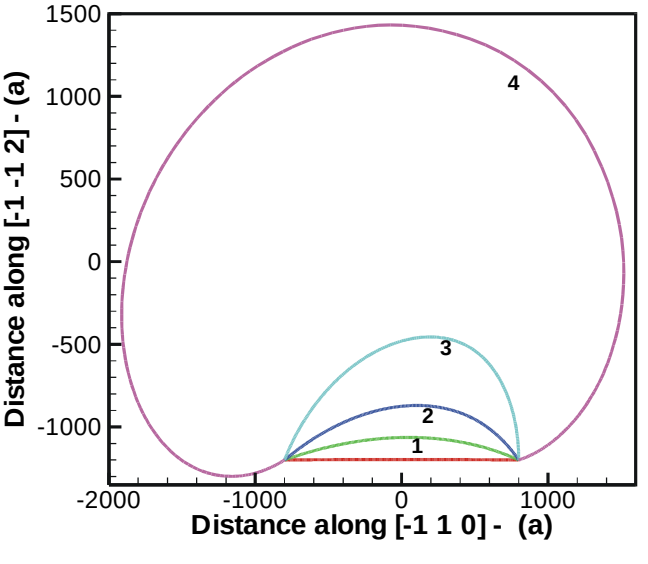

Fig. (3): Response of an F-R source to a stress ramp slower than 1 MPa / ps. All conditions are of the same as Fig. (2). (1) at 50 MPa ($\frac{t}{m} = 0.041\%$), (2) 100 MPa ($\frac{t}{m} = 0.082\%$), (3) 150MPa ($\frac{t}{m} = 0.122\%$), (4) 200 MPa ($\frac{t}{m} = 0.163\%$) - unstable state.

21 cubic spline segments have been used in the simulations, with as few as 3 segments giving sufficient accuracy [14]. The EOM have been implicitly integrated for stability at a relative accuracy of 10^{-5}, using Gear's methods for stiff, ordinary differential equations [17]. While the response of the F-R source to low stress impact-type loading results in an equilibrium shape within tens of picoseconds, Fig. (3) shows the F-R source evolution following a stress ramp with a stress rate slower than 1 MPa/ ps. The conditions of Fig. (3) are the same as in Fig. (2), except that in this case the F-R source develops in a quasi-equilibrium fashion to adjust to the instantaneous stress till it becomes unstable at σ_{11} = 200 MPa ($\frac{t}{m} = 0.163\%$). The self-force is not restraining any more at this stress level, and the F-R source expands without additional increase in the applied stress. The dislocation line acts like a string that is stiffer in the screw orientation than the edge orientation, and thus stretches along $\mathbf{b} = \left[\bar{1}01\right]$. The degree of such asymmetric deformation depends on the stress rate and its magnitude in relationship to the self-force, but it is always observed in the simulations.

Once the F-R source is unstable, it will continue its expansion till the opposite arms come within one Burgers vector, at which instant node rearrangements take place in the simulations, and a new loop is formed. Fig. (4) shows the dynamics of this short-range annihilation reaction and the ensuing relaxation of the asymmetric cusp on the freshly generated loop. The simulation is carried out for the same conditions as in Figs. (2&3) except the Burgers vector $\mathbf{b} = \frac{1}{2}\left[\bar{1}01\right]$ at an impact stress σ_{11} =100 MPa. Generation of the fresh loop is achieved at 28.3 ns.

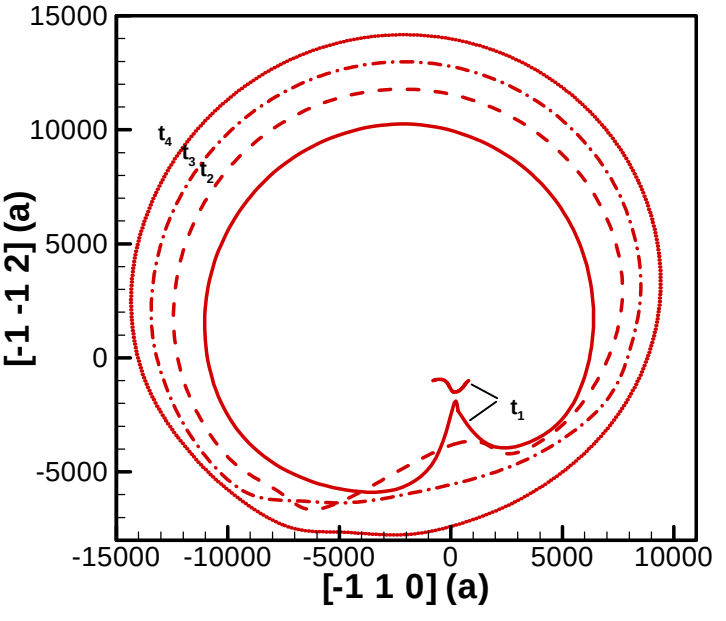

Fig. (4) Dynamics of the short-range annihilation reaction and its subsequent relaxation for an F-R source on the (111) plane. The time intervals are t_1= 28.3, t_2= 30.8, t_3= 31.8, t_4= 32.8 ns, respectively.

3.2 Finite-Size Dipoles

Nucleation and break-up of dislocation dipoles appears to play a significant role in the evolution of Persistent Slip Bands (PSBs) under conditions of fatigue loading [18]. Unlike 2-D simulations where additional rules were invoked for the process of formation and destruction of such dipoles [e.g. 18], Fig. (5) illustrates the natural time evolution of a finite-size dipole. In this case, two parallel straight segments lying on parallel (111) planes are pinned on both ends, and separated by an inter-planar distance of $z = 40\sqrt{3}a$. Both dislocations are intially of mixed character, with have $\mathbf{b} = \left[\bar{1}01\right]$ and tangent vectors of opposite directions along $\left[\bar{1}10\right]$. Each dislocation was divided into 5 curved

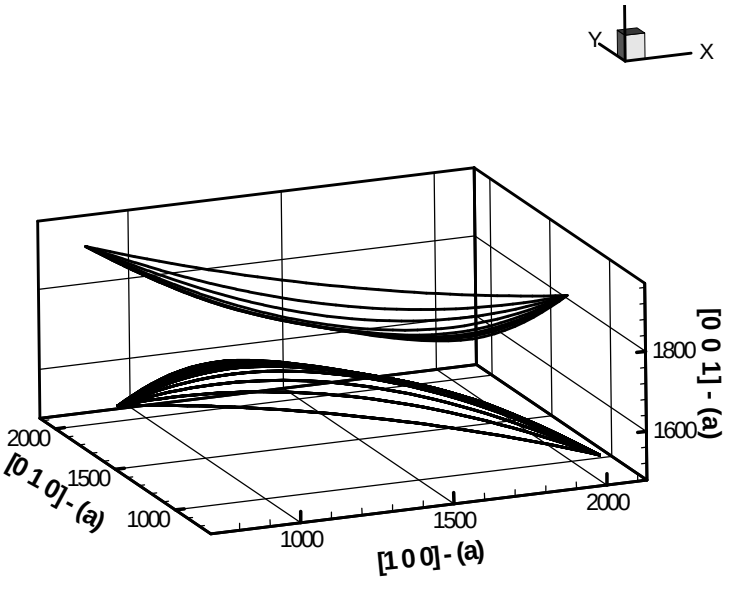

Fig. (5) Finite-size dipole formation without applied stress. The dipole is composed of two parallel segments on (1 1 1) planes, separated by an inter-planar distance of $\sqrt{\ }$ with **b**=[-1 0 1].

segments and represented by cubic splines, and allowed to interact and deform without an externally applied stress. As a result of their mutual interaction, the two dislocations attract one another till they form a middle mixed-character dipole section that is nearly straight. The length of the middle dipolar section is only limited by the line tension as a result of curvatures formed during the evolution process. An external stress is then applied on the dipole to determine the conditions for its destruction. When the direction of the stress is such that the two dislocations move past one another (forward motion), a relatively high level of stress is required to breakup the dipole, because it must also overcome developed line tensions, as can be seen from Fig. (5). The required value of the stress in this case is σ_{11} =250 MPa ($\frac{t}{m} = 0.2\%$). On the other hand, when the stress direction is reversed, the motion of the two dislocations is assisted by the line tension, and the required stress is significantly lower. Scaling relationships for dipole break-up stress are developed in reference [14].

3.4 Dislocation Junctions

2-D simulations have shown that dislocation junctions stabilize cell structures [18]. However, junction rules were introduced as a result of the limitations of 2-D simulations. Additionally, strain hardening as determined by forest interaction mechanisms is dictated primarily by the intrinsic junction strength. In the PDD technique, junction formation and destruction is treated in exactly the same manner as finite dipoles, with the simple limitation that dislocation cores are not allowed to interpenetrate. Thus, no special rules are required to study the stability and dynamics of junctions. Once attractive segments belonging to different dislocations approach one another, the two participating segments are stopped when the distance between them ≤ b. Fig. (7) shows several stages for the evolution of an attractive dislocation junction in FCC metals, formed by the interaction of two F-R sources operating on two intersecting (111)-type planes. The first F-R source is: $\frac{1}{2}\left[\bar{1}01\right]\left(1\bar{1}1\right)$, while the second is given by: $\frac{1}{2}\left[1\bar{1}0\right]\left(11\bar{1}\right)$. In these simulations, the number of segments on each F-R source was varied between 4 and 8, giving indistinguishable results for the evolution dynamics and critical breakup stress. Computer simulations indicate that attractive junctions can form extremely fast, within tens of ps, as can be seen for the final equilibrium state of an unstressed attractive junction in Fig. (7-a). On the other hand, significant applied stress is necessary to partially unzip the junction, as can be ascertained from Fig. (7-b) at σ_{11} = -50 MPa ($\frac{t}{m} = 0.0408\%$), where the final equilibrium configuration of the junction at this stress is shown. Fig. (7-c) shows the equilibrium configuration of a totally destroyed (separated) junction at an increased applied stress of σ_{11} = - 100 MPa ($\frac{t}{m} = 0.082\%$). The two glide planes are symmetric with respect to the uniaxial applied stress, with identical CRSS acting on each. While the unstressed junction in Fig. (7-a) is stable under the equilibrium of attractive forces along their common section and the self-forces on their curved arms, quasi-static unzipped configurations in Fig. (7-b) are stabilized with the additional external cumulative forces. When the influence of external forces exceeds a critical value (junction strength), a fully

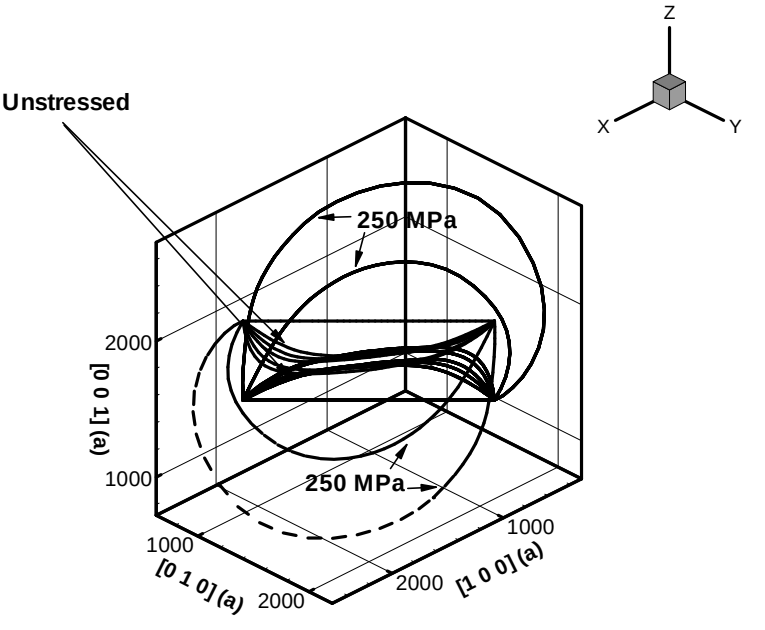

Fig. (6): Dynamic evolution for forward break-up of a mixed-character finite-size dipole in FCC metals on the (11) plane.

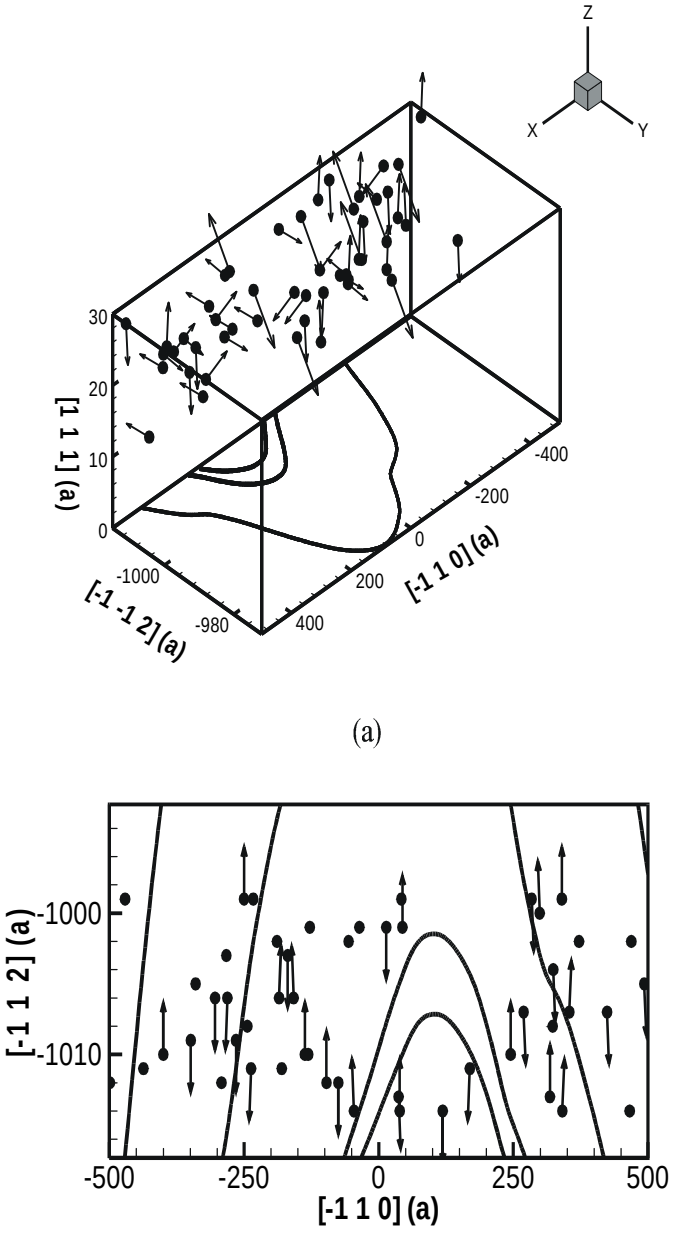

Fig. (8): Dynamic interaction between an F-R source and a random atmosphere of 50 sessile SIA dislocation loops near the glide plane. SIA loops have a random distribution of size, space and Burgers vector (shown by arrows). F-R $\mathbf{b} = \frac{1}{2}[\bar{1}01]$:

(a) 3-D positions, and (b) motion projection on the (111) plane.

unzipped configuration is evolved, as can be seen in Fig. (7-c). It is interesting to note here that very few curved segments are sufficient to capture this type of strong short-range interaction.

3.5 Interaction with Defect Clusters

Irradiation-induced defect clusters are responsible for radiation hardening and the onset of plastic instability. We consider here the interaction between the F-R source and 50 prismatic self-interstitial atom (SIA) dislocation loops in an *atmosphere*. The cluster atmosphere is contained in the parallelepiped

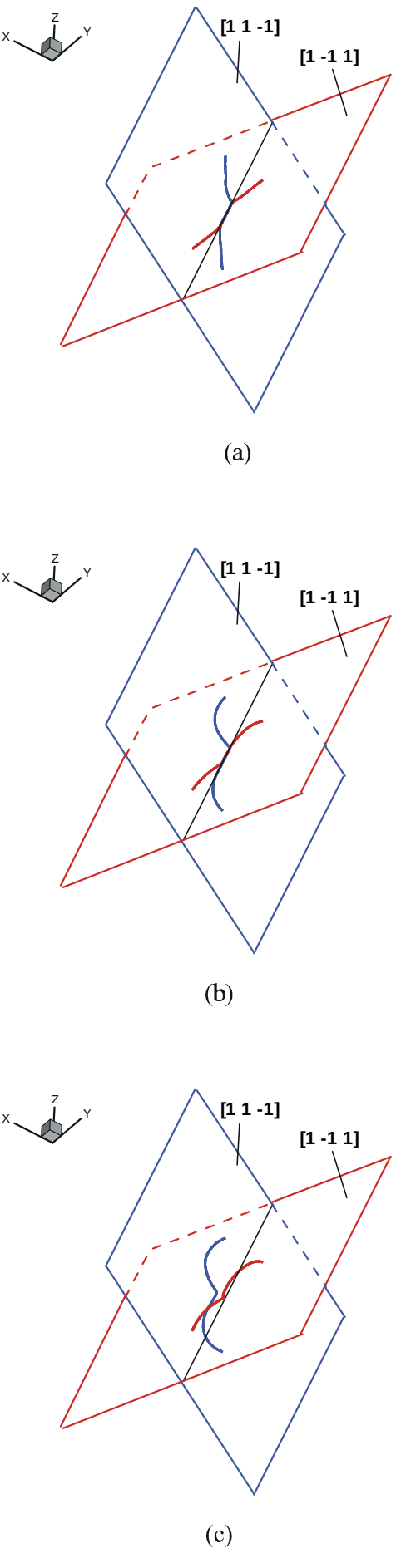

Fig. (7): Formation (a), unzipping (b) and destruction of an attractive junction in FCC metals.

bounded by: (-500 a ≤x ≤ 500 a), (-1015 a ≤y ≤ -1000 a), and (15 a ≤z ≤30 a). Defect clusters here are assumed to have random Burgers vectors, selected from the set: **b**= 1/2 [110], and are given random locations within the parallelepiped. Fig. (8) shows the interaction dynamics between an F-R source expanding against the influence of the collective force of a cluster atmosphere. The applied shear stress is increased by 4 MPa intervals, and the dislocation shape is evolved till it reaches an equilibrium configuration, up to a stress level of 36 MPa. It is noted that the dislocation line shape changes significantly as it approaches the SIA cluster atmosphere. The continuously smooth line becomes highly curved in the vicinity of the cluster atmosphere. As the applied shear stress increases to a critical value (40 MPa), the dislocation line flattens and develops incipient fluctuations. Finally, morphological shape instabilities in the middle section of the F-R source enable the F-R source dislocation to penetrate through the cluster elastic field. Fig. (8-a) shows 3-D positions of 50 SIA clusters and the interacting dislocation line position at various time intervals, while the projection of clusters and the dislocation on the glide plane is depicted in Fig. (8-b). Cluster radii in this atmosphere are in the range: 3-5 a, and their position and Burgers vector are both randomly selected.

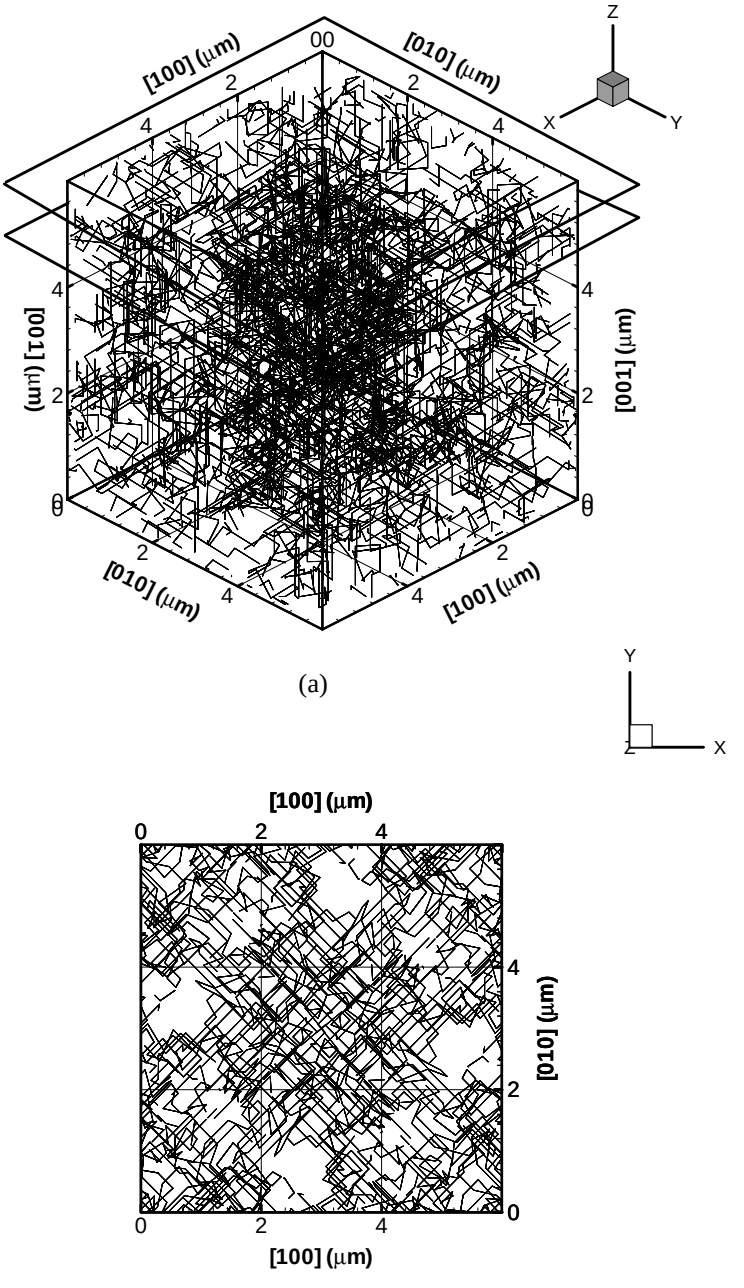

Fig. (9): Random dislocation loop distribution with the Periodic Boundary Condition (PBC) in FCC crystals. Loop segments, which emerge from one slip system, are reintroduced in the RVE by periodic mapping.

3.6 Boundary Conditions

Two types of boundary conditions have been developed for the PDD method. A superposition method has been used for free surfaces (i.e. image forces) by combining the elastic field of residual surface tractions, computed by the FEM technique, with the field generated by parametric dislocations (e.g. Eqn. 1) [19]. On the other hand, translational strain invariance has led to the development of a special Periodic Boundary Condition (PBC) for simulations of small Representative Volume Elements (RVEs), which can be used to obtain information on spatial distributions of the microstructure or on constitutive relations. In the PBC, dislocation loops are generated with segments lying on randomly selected slip planes, and the segments are connected with sessile superjogs so as to ensure mechanical equilibrium for closed loops. If a part of the loop is detected to be outside the RVE, the parametric position vector is mapped periodically onto the RVE. This technique preserves translational strain invariance and mechanical equilibrium, and

solves the problem of artificial dislocation depletion at the simulation boundaries. A dislocation microstructure obtained with this method is shown in Fig. (9-a), together with a TEM slice in Fig. (9-b).

4. CONCLUSIONS

Recent developments in the PDD method for computer simulations of mesoscopic plastic deformation have been reviewed in this article. The following encouraging features of the method have been revealed: (1) development of new and convenient vector forms for the elastic field of dislocations; (2) accurate and stable interaction dynamics of all short-range reactions without additional ad hoc assumptions; (3) resolution of spatial and temporal interaction events with a few generalized DOFs; (4) implementation of self-consistent boundary conditions for free surfaces, and for RVEs. Nevertheless, challenging questions remain ahead before full and reliable utilization of the method can finally be achieved. These are: (1) extensions to anisotropic elastic media at a reasonable computational cost; (2) rigorous and efficient implementation of the superposition principle for PDD with the FEM technique; (3) a rigorous methodology for approximating the far field of dislocations to avoid N^2 interactions; (4) elasto-plastic formulation with finite lattice rotations; (5) dislocation interaction with surface steps; and (6) applications to material design for systems of optimized strength and ductility.

Acknowledgements

Support of he US Department of Energy, Office of Fusion Energy of this research through grants: DE-FG03-98ER54500 (radiation embrittlement) and DE-FG03-00ER54594 (laser-material interaction) with UCLA is gratefully acknowledged.

References

[1] L.P Kubin, and G. Canova, *Scr. Metall*. **27** (1992) 957.
[2] B. Devincre, and M. Condat, *Acta Metall. Mater* **40**(1992) 2629.
[3] L.P. Kubin, *Phys. Status Solidi (a)* **135**(993) 433 .
[4] J.P. Hirth, M. Rhee, and H.M. Zbib, *J. Computer-Aided Mater. Design* **3**(1996) 164.
[5] K.W. Schwarz, *Phys. Rev. Lett.* **78**(1997) 4785.
[6] R. Sedlacek, *Phil. Mag. Lett.* **76:(4)**(1997) 275 .
[7] H.M. Zbib, M. Rhee, and J.P.Hirth, *Inter. J. Mech. Sci.* **40**(1998) 113.
[8] K.W. Schwarz, *J. Appl. Phys*., 85(1999) 108.
[9] N.M. Ghoniem, *J. Eng. Mater. Tech*. **121**(1999) 136.
[10] N.M. Ghoniem, L.Z. Sun, *Phys. Rev. B* **60**(1999) 128.
[11] Multiscale Modeling of Materials, Materials Research Society (MRS) Symposium Proceedings, Boston, MA. , U.S.A., Nov. 1998, V.V. Bulatov, T. Diaz de la Rubia, R. Phillips, E. Kaxiras, and N.M. Ghoniem, Editors, MRS Publication, Warrendale, PA. **538** (1999).
[12] N.M. Ghoniem, S-.S Tong, and L.Z., Sun, *Phys. Rev. B* **61(1)**(2000) 913.
[13] N.M. Ghoniem, B. N. Singh, L. Z. Sun, and T. Diaz de la Rubia, *J. Nucl. Mater*, **276** (2000) 166.
[14] J. Huang, and N.M. Ghoniem "Space and Time Resolution of Parametric Dislocation Dynamics," to be submitted, *Phys. Rev. B*, (2001).
[15] N.M. Ghoniem and J. Huang, "Differential Triplet Vector Forms for the Elastic Field of Parametric Dislocations," *Phil. Mag. Lett*., to be submitted, (2001).
[16] J.M. Burgers, *Proc. Koninkl. Ned. Akad. Wetenschap*. **42**(1939) 293.
[17] C.W. Gear, Numerical initial value problems in ordinary differential equations, Prentice-Hall, Englewood Cliffs, N.J., 1971.
[18] R. J. Amodeo and N. M. Ghoniem, *Phys. Rev.* **B41** (1990) 6968.
[19] R. Martinez, M.S. Thesis, UCLA, July 2000, also R. Martinez and N. Ghoniem, " The Influence of Crystal Surfaces on Dislocation Interactions in Mesoscopic Plasticity: A Combined Dislocation Dynamics - Finite Element Approach ," presented at the International Conference on Computational Engineering Sciences (ICES2K), Anahiem, CA., August 2000.